Available online at www.sciencedirect.com
SCIENCE DIRECT®
Composites Science and Technology 64 (2004) 2393–2406
COMPOSITES SCIENCE AND TECHNOLOGY
www.elsevier.com/locate/compscitech

Beam and finite element analysis of quasi-unidirectional composite SLB and ELS specimens

András Szekrényes *, József Uj [1]

Department of Applied Mechanics, Budapest University of Technology and Economics, P.O. Box 11, H-1521 Budapest, Hungary

Received 10 November 2003; received in revised form 4 May 2004; accepted 5 May 2004
Available online 25 June 2004

Abstract

The mixed-mode I/II delamination problem in composite specimens was investigated using closed-from solutions, the finite element technique and experiments. Unidirectional glass/polyester composite laminates were manufactured and tested. The mixed-mode I/II SLB and ELS specimen configurations were used in order to obtain compliance and fracture energy predictions. Linear beam theories incorporating transverse shear and elastic foundation effects were utilized to calculate the displacements of both the SLB and ELS specimens. The compliance and fracture energy was calculated as the superposition of the various contributions. Plane stress finite element models including some accompanying effects were constructed. The analytical and numerical results were compared with the experiments and very good agreement was found.

Keywords: B. Fracture toughness; Timoshenko beam theory

1. Introduction

Interlaminar fracture tests are carried out on configurations in which the specimens behave as slender beams. The standard double-cantilever beam (DCB) specimen is a well-established tool for measuring the mode-I fracture toughness. Advanced beam models of the DCB specimen were developed based on Winkler foundation analysis in [1,2]. For mode-II testing the end-notched flexure (ENF), the four-point bend end-notched flexure (4ENF) and the mode-II end-loaded split (ELS) configurations are available. Wang and Williams [3] provided corrections for the ENF and mode-II ELS specimens using three numerical schemes and good agreement was found. The ENF specimen was discussed in detail by Ozdil et al. [4] and Carlsson et al. [5] incorporating transverse shear and frictional effects. Schuecker and Davidson [6] shown, that if the crack length and the compliance are measured accurately, the ENF and 4ENF tests give the same fracture toughness values. Hashemi et al. [7,8] investigated carbon/PEEK and polyether-sulphone (PES) fiber composites using the DCB, mode-II ELS and the mixed-mode I/II ELS specimens. Considering mixed-mode I/II configurations the most effective one is the standard mixed-mode bending (MMB), which enables the variation of the mode ratio. Ozdil and Carlsson [9] used this apparatus for testing glass/polyester laminates. The compliance and fracture energy equations based on beam theories can be found in other works [10,11]. Despite the MMB is widely accepted for testing unidirectional laminates, a number of works investigate other type of mixed-mode configurations. Reyes and Cantwell [12] referred to the mixed-mode I/II ELS specimen as single-cantilever beam (SCB). The ELS configurations were discussed using simple beam theory [13] and finite element method [14] by others. Another mixed-mode I/II test is the

* Corresponding author. Tel.: +36-1-463-1170; fax: +36-1-463-3471.
E-mail addresses: szeki@mm.bme.hu (A. Szekrényes), uj@mm.bme.hu (J. Uj).
[1] Tel.: +36-1-463-2228; fax: +36-1-463-3471.

0266-3538/$ - see front matter © 2004 Elsevier Ltd. All rights reserved.
doi:10.1016/j.compscitech.2004.05.002

single-leg bending (SLB), which was proposed by Yoon and Hong [15] as a modified ENF specimen. A large number of theoretical and experimental works were performed by Davidson et al. [16–19] about the SLB specimen. Davidson and Koudela [20] examined also the effect of precracking mode on the fracture toughness using DCB, ENF and SLB coupons. Later the SLB test was modified by Tracy et al. [21] and the single leg four point bend (SLFPB) specimen was introduced. The mixed-mode flexure (MMF) specimen was applied by Albertsen et al. [22] and by Korjakin et al. [23]. Finally the cracked-lap shear (CLS) specimen should be mentioned [22,24].

In the present work quasi-unidirectional $[0°]_{14}$ mixed-mode I/II SLB and ELS specimens are analysed using linear beam theories, finite element method and experiments. Although these tests are not as universal as the MMB, they require more simple experimental equipment. The latter requires complex fixture and steel hinge tabs. The SLB test may be performed in a simple three-point bending setup, while the mixed-mode I/II ELS specimen requires a clamping fixture. The SLB and ELS tests produce linear load-deflection curve up to fracture and simple reduction techniques can be applied. We note that the name ELS is reserved for the mode-II version of this test, but we still prefer this name and will refer to the mixed-mode version of this specimen as ELS. Fig. 1 illustrates the mixed-mode I/II specimen configurations and geometry parameters.

2. Beam analysis—compliance and fracture energy

2.1. Analysis of the SLB specimen

The SLB geometry is depicted in Fig. 2. The compliance can easily be obtained based on the work of Ozdil et al. [4], wherein the following expression was derived for the ENF specimen using Timoshenko beam theory

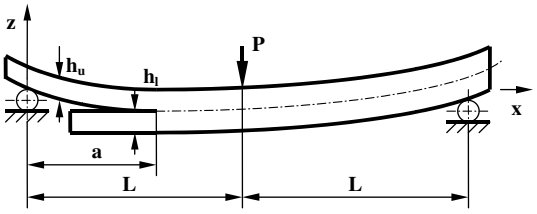

Fig. 2. Delaminated and uncracked regions of the SLB specimen.

$$C=\left[\frac{2L^3d_{11,2}+a^3(d_{11,1}-d_{11,2})}{12}+\frac{2La_{55,2}+a(a_{55,1}-a_{55,2})}{4k}\right], \tag{1}$$

where $k=5/6$ is the shear correction factor. The fracture toughness can be expressed by differentiating the compliance with respect to crack length [25]

$$G_{\mathrm{I/II}}=\frac{P^2}{2b}\frac{\mathrm{d}C}{\mathrm{d}a}. \tag{2}$$

Thus we obtain

$$G_{\mathrm{I/II}}=\frac{P^2}{8b}\left[a^2(d_{11,1}-d_{11,2})+\frac{(a_{55,1}-a_{55,2})}{k}\right]. \tag{3}$$

The differences between the ENF and SLB specimens are the distinct shear and bending compliances of the delaminated region. Using the equations in Appendix A, Eqs. (1) and (3) can be simplified.

2.2. Analysis of the mixed-mode I/II ELS specimen

2.2.1. Winkler foundation analysis

The elastic foundation model (EFM) is illustrated in Fig. 3. The model consists of two beams, which are connected with the linear springs along the uncracked region. Four deflection functions are necessary to model the whole specimen, as shown in Fig. 3. A detailed view at the crack tip zone is also given at the bottom of Fig. 3. The deflection functions of the upper and lower arms are:

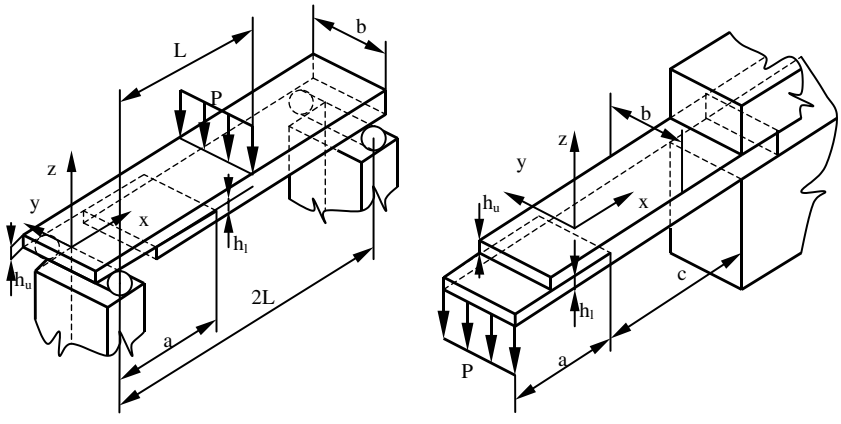

(a) **S**ingle **L**eg **B**ending Specimen (**SLB**) **(b)** **E**nd **L**oaded **S**plit Specimen (**ELS**)

Fig. 1. Mixed-mode I/II test configurations: (a) single leg bending (SLB) specimen; (b) end loaded split (ELS) specimen.

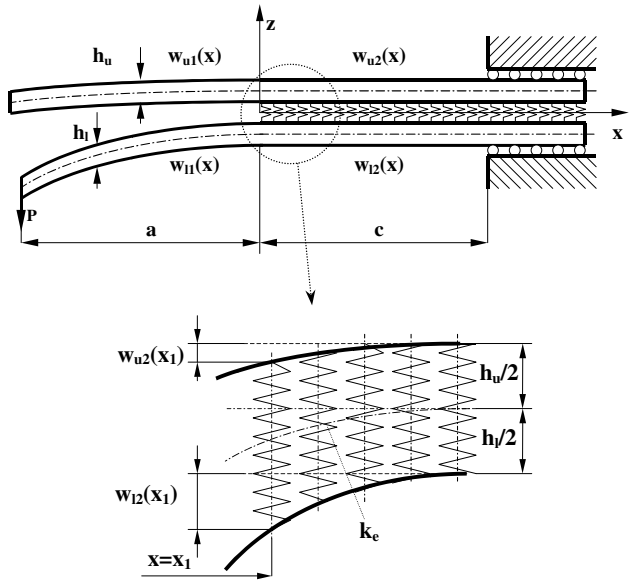

Fig. 3. Winkler foundation model for the ELS specimen.

$$w_{u1}(x) = c_1 + c_2 x, \quad -a \leqslant x \leqslant 0, \tag{4}$$

$$w_{l1}(x) = \frac{-P}{I^{l}_{y1} E_{11}}\left[\frac{x^3}{6} + \frac{a x^2}{2}\right] + c_3 x + c_4, \quad -a \leqslant x \leqslant 0, \tag{5}$$

where I^{l}_{y1} is the second order moment of inertia of the lower arm in the cracked region. Based on Fig. 3 the potential energy of the uncracked region can be formulated as

$$U = \frac{1}{2}\int I^{u}_{y2} E_{11} w''_{u2}(x)^2 \mathrm{d}x + \frac{1}{2}\int I^{l}_{y2} E_{11} w''_{l2}(x)^2 \mathrm{d}x + \frac{1}{2}\int k_e (w_{u2}(x) - w_{l2}(x))^2 \mathrm{d}x, \tag{6}$$

where I^{u}_{y2} and I^{l}_{y2} are the second order moments of inertia of the upper ($w_{u2}(x)$) and lower ($w_{l2}(x)$) sub-beams in the uncracked region and k_e is the extensional modulus. Stationarity of the functional in Eq. (6) involves the following differential equations for the deflection functions $w_{u2}(x)$, $w_{l2}(x)$:

$$I^{l}_{y2} E_{11} \frac{\mathrm{d}^4 w_{l2}(x)}{\mathrm{d}x^4} + k_e w_{l2}(x) = k_e w_{u2}(x), \qquad 0 \leqslant x \leqslant c,$$
$$I^{u}_{y2} E_{11} \frac{\mathrm{d}^4 w_{u2}(x)}{\mathrm{d}x^4} + k_e w_{u2}(x) = k_e w_{l2}(x), \qquad 0 \leqslant x \leqslant c. \tag{7}$$

We first define the foundation moduli k_e. The elastic strain in the transverse direction is (see Fig. 3)

$$\varepsilon_z = \frac{w_{l2}(x) - w_{u2}(x)}{h}, \tag{8}$$

where $h = (h_u + h_l)/2$. According to Ozdil and Carlsson [2] the foundation moduli is

$$k_e = \frac{b\sigma_z(x)}{w_{l2}(x) - w_{u2}(x)}. \tag{9}$$

Using the one-dimensional Hooke's law we obtain

$$\sigma_z(x) = E_{33}\varepsilon_z. \tag{10}$$

Combining Eqs. (8)–(10) yields

$$k_e = \frac{bE_{33}}{h}. \tag{11}$$

Substituting Eq. (11) into (7) the governing equations of the deflections are:

$$\frac{\mathrm{d}^4 w_{l2}(x)}{\mathrm{d}x^4} + 4\beta_l^4 w_{l2}(x) = 4\beta_l^4 w_{u2}(x), \quad 0 \leqslant x \leqslant c,$$
$$\frac{\mathrm{d}^4 w_{u2}(x)}{\mathrm{d}x^4} + 4\beta_u^4 w_{u2}(x) = 4\beta_u^4 w_{l2}(x), \quad 0 \leqslant x \leqslant c, \tag{12}$$

where

$$\beta_l = \left(\frac{3}{h h_l (h_l^2 + 3h_u^2)}\right)^{1/4}\left(\frac{E_{33}}{E_{11}}\right)^{1/4},$$
$$\beta_u = \left(\frac{3}{h h_u (h_u^2 + 3h_l^2)}\right)^{1/4}\left(\frac{E_{33}}{E_{11}}\right)^{1/4}. \tag{13}$$

The solution of Eq. (12) can be obtained by combining the Krulov-functions [26] and adding a third order polynomial, as given in Appendix B. The parameters [c_1–c_{12} in Eqs. (4), (5), (B.2a) and (B.2b)] can be calculated by using the boundary and matching conditions (also given in Appendix B). Using Steiner's theorem the second order moments of inertia are:

$$I^{u}_{y1} = \frac{b h_u^3}{12}, \quad I^{u}_{y2} = \frac{b h_u (h_u^2 + 3h_l^2)}{12},$$
$$I^{l}_{y1} = \frac{b h_l^3}{12}, \quad I^{l}_{y2} = \frac{b h_l (h_l^2 + 3h_u^2)}{12}. \tag{14}$$

Notice that Eq. (13) was obtained by the help of Eq. (14). The compliance ($Cw_{l1}(-a)/P$) can be simplified by assuming that $c \gg h$, where h is half of the specimen thickness. We consider only the case of symmetric specimen. When $h_u = h_l = h$, then the compliance becomes

$$C_W = \frac{7a^3 + L^3}{2bh^3 E_{11}} + \frac{a^3}{2bh^3 E_{11}}\left[2.71\left(\frac{h}{a}\right)\left(\frac{E_{11}}{E_{33}}\right)^{1/4} + 2.45\left(\frac{h}{a}\right)^2\left(\frac{E_{11}}{E_{33}}\right)^{1/2} + 1.11\left(\frac{h}{a}\right)^3\left(\frac{E_{11}}{E_{33}}\right)^{3/4}\right], \tag{15}$$

where $L = a + c$ is the full length of the specimen. Combining Eqs. (15) and (2) yields

$$G_{\mathrm{W,I/II}} = \frac{21P^2a^2}{4b^2h^3E_{11}} + \frac{P^2a^2}{4b^2h^3E_{11}}\left[5.42\left(\frac{h}{a}\right)\left(\frac{E_{11}}{E_{33}}\right)^{1/4} + 2.45\left(\frac{h}{a}\right)^2\left(\frac{E_{11}}{E_{33}}\right)^{1/2}\right]. \quad (16)$$

2.2.2. Timoshenko beam theory

The application of Timoshenko beam theory [4] results in the following expressions in the case of the ELS specimen:

$$C_{\mathrm{T}} = \frac{7a^3 + L^3}{2bh^3E_{11}} + \frac{a+L}{2bhkG_{13}}, \quad (17)$$

$$G_{\mathrm{T,I/II}} = \frac{21P^2a^2}{4b^2h^3E_{11}} + \frac{P^2}{4b^2hkG_{13}}. \quad (18)$$

2.2.3. Saint Venant effect

The Saint Venant effect was analysed by Olsson [1] for the DCB specimen. The solution in [1] was originally provided by Horgan [27]. According to Olsson's analysis the compliance contribution has the following form in the case of the ELS specimen:

$$C_{\mathrm{SV}} = \frac{3}{\pi}\frac{L^2}{bh^2E_{11}}\left(\frac{E_{11}}{G_{13}}\right)^{1/2}. \quad (19)$$

2.3. Summary of the compliance and fracture energy contributions

Based on Section 2.2.1 similar equations can be derived for the SLB specimen. Superposing the transverse shear and elastic foundation effects the compliance of the SLB specimen becomes:

$$C^{\mathrm{SLB}} = \frac{7a^3 + 2L^3}{8bh^3E_{11}} + \frac{a+2L}{8bhkG_{13}} + \frac{a^3}{8bh^3E_{11}} \times \left[2.71\left(\frac{h}{a}\right)\left(\frac{E_{11}}{E_{33}}\right)^{1/4} + 2.45\left(\frac{h}{a}\right)^2\left(\frac{E_{11}}{E_{33}}\right)^{1/2} + 1.11\left(\frac{h}{a}\right)^3\left(\frac{E_{11}}{E_{33}}\right)^{3/4}\right]. \quad (20)$$

Note that Eq. (1) was simplified using the equations in Appendix A and implemented into Eq. (20). The fracture toughness can be calculated by using Eq. (2)

$$G^{\mathrm{SLB}}_{\mathrm{I/II}} = \frac{21P^2a^2}{16b^2h^3E_{11}} + \frac{P^2}{16b^2hkG_{13}} + \frac{P^2a^2}{16b^2h^3E_{11}} \times \left[5.42\left(\frac{h}{a}\right)\left(\frac{E_{11}}{E_{33}}\right)^{1/4} + 2.45\left(\frac{h}{a}\right)^2\left(\frac{E_{11}}{E_{33}}\right)^{1/2}\right]. \quad (21)$$

As the superposition of Eqs. (15) and (17) the compliance of the ELS specimens is

$$C^{\mathrm{ELS}} = \frac{7a^3+L^3}{2bh^3E_{11}} + \frac{a+L}{2bhkG_{13}} + \frac{3}{\pi}\frac{L^2}{bh^2E_{11}}\left(\frac{E_{11}}{G_{13}}\right)^{1/2} + \frac{a^3}{2bh^3E_{11}}\left[2.71\left(\frac{h}{a}\right)\left(\frac{E_{11}}{E_{33}}\right)^{1/4} + 2.45\left(\frac{h}{a}\right)^2\left(\frac{E_{11}}{E_{33}}\right)^{1/2} + 1.11\left(\frac{h}{a}\right)^3\left(\frac{E_{11}}{E_{33}}\right)^{3/4}\right]. \quad (22)$$

The fracture energy is given by

$$G^{\mathrm{ELS}}_{\mathrm{I/II}} = \frac{21P^2a^2}{4b^2h^3E_{11}} + \frac{P^2}{4b^2hkG_{13}} + \frac{P^2a^2}{4b^2h^3E_{11}} \times \left[5.42\left(\frac{h}{a}\right)\left(\frac{E_{11}}{E_{33}}\right)^{1/4} + 2.45\left(\frac{h}{a}\right)^2\left(\frac{E_{11}}{E_{33}}\right)^{1/2}\right]. \quad (23)$$

2.4. Mode-mixity analysis

In literature several mode-partitioning methods are available. Ducept et al. [28] applied Williams' [29] method based on simple beam theory and another one based on the work of Suo and Hutchinson [30]. These methods give the same results in the case of symmetric specimens. The former methods were used in other works [24,31]. Sundararaman and Davidson [32,33] applied crack tip element (CTE) analysis, which is equivalent to the method developed by Suo and Hutchinson.

Here Williams' method was adopted and improved with the effect of transverse shear and Winkler foundation. Only unidirectional specimens with midplane crack are considered here.

2.4.1. Mode partitioning using beam theories

Let us see the problem in Fig. 4(a). Superposing the effects of transverse shear and elastic foundation based on Sections 2.1 and 2.2 the compliance of the upper (1) and lower (2) arms are:

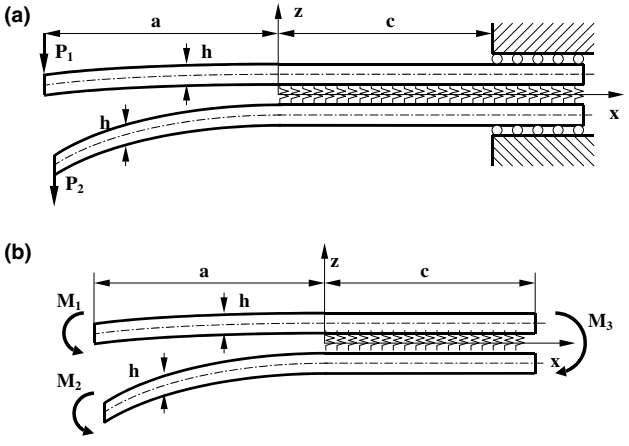

Fig. 4. Reduction scheme for mixed-mode partitioning.

$$C_1 = \frac{7a^3 + L^3}{2bh^3E_{11}} + \frac{(L^3 - a^3)P_2}{2bh^3E_{11}P_1} + \frac{L(P_1 + P_2) + a(P_1 - P_2)}{bhkG_{13}P_1} + \frac{a^3(P_1 - P_2)}{2bh^3E_{11}P_1} f_{W1}, \tag{24}$$

$$C_2 = \frac{7a^3 + L^3}{2bh^3E_{11}} + \frac{(L^3 - a^3)P_1}{2bh^3E_{11}P_2} + \frac{L(P_1 + P_2) + a(P_2 - P_1)}{bhkG_{13}P_2} + \frac{a^3(P_2 - P_1)}{2bh^3E_{11}P_2} f_{W1}, \tag{25}$$

where

$$f_{W1} = 2.71\left(\frac{h}{a}\right)\left(\frac{E_{11}}{E_{33}}\right)^{1/4} + 2.45\left(\frac{h}{a}\right)^2\left(\frac{E_{11}}{E_{33}}\right)^{1/2} + 1.11\left(\frac{h}{a}\right)^3\left(\frac{E_{11}}{E_{33}}\right)^{3/4}. \tag{26}$$

The fracture energies yield by using Eq. (2):

$$G_1 = \frac{21P_1^2a^2}{4b^2h^3E_{11}} - \frac{3P_1P_2a^2}{4b^2h^3E_{11}} + \frac{P_1(P_1 - P_2)}{4b^2hkG_{13}} + \frac{P_1(P_1 - P_2)a^2}{4bh^3E_{11}} f_{W2}, \tag{27}$$

$$G_2 = \frac{21P_2^2a^2}{4b^2h^3E_{11}} - \frac{3P_1P_2a^2}{4b^2h^3E_{11}} + \frac{P_2(P_2 - P_1)}{4b^2hkG_{13}} + \frac{P_2(P_2 - P_1)a^2}{4bh^3E_{11}} f_{W2}, \tag{28}$$

where

$$f_{W2} = 5.42\left(\frac{h}{a}\right)\left(\frac{E_{11}}{E_{33}}\right)^{1/4} + 2.45\left(\frac{h}{a}\right)^2\left(\frac{E_{11}}{E_{33}}\right)^{1/2}. \tag{29}$$

According to Fig. 4 we reduce problem (a) into problem (b), where $M_1 = P_1a$, $M_2 = P_2a$, and $M_3 = M_1 + M_2$ are bending moments at the crack tip. The sum of Eqs. (27) and (28) can be transformed as

$$G_T = \frac{21(M_1^2 + M_2^2) - 6M_1M_2 + (M_1 - M_2)^2(f_T + f_{W2})}{4b^2h^3E_{11}}, \tag{30}$$

where

$$f_T = \frac{1}{k}\frac{E_{11}}{G_{13}}\left(\frac{h}{a}\right)^2. \tag{31}$$

According to Ducept et al. [28] the equivalent bending moments can be decomposed as:

$$M_1 = M_I + M_{II}, \quad M_2 = \alpha M_I + \varphi M_{II}. \tag{32}$$

In the case of pure mode-II the upper and lower specimen arms have the same curvature

$$\frac{12M_{II}}{bh^3E_{11}} = \frac{12\varphi M_{II}}{bh^3E_{11}}. \tag{33}$$

From which yields that $\phi = 1$. Substituting Eq. (32) into (30) allows separation of the term containing the product of M_IM_{II}

$$G^*_{I/II} = \frac{9M_IM_{II}(1 + \alpha)}{b^2h^3E_{11}}. \tag{34}$$

In order to cancel this term we choose $\alpha = -1$. Then the mode-I and mode-II components are:

$$G_I = \frac{M_I^2(12 + f_T + f_{W2})}{b^2h^3E_{11}}, \tag{35}$$

$$G_{II} = \frac{9M_{II}^2}{b^2h^3E_{11}}. \tag{36}$$

Rearranging Eq. (32) we obtain

$$M_I = (M_1 - M_2)/2, \quad M_{II} = (M_1 + M_2)/2. \tag{37}$$

According to Eqs. (35) and (36) transverse shear and elastic foundation contributes only to the mode-I component. The former can be explained by the fact, that transverse shear does not change the curvatures of the unidirectional specimen arms. On the other hand it is obvious that elastic foundation supports only the mode-I component, as shown by Ozdil and Carlsson [9].

2.4.2. Application to the SLB and ELS specimens

For the SLB specimen the reduced bending moments at the crack tip are: $M_1 = 0, M_2 = Pa/2$. Using Eqs. (35) and (36) the energy release rate components are:

$$G_I^{SLB} = \frac{12P^2a^2}{16b^2h^3E_{11}} + \frac{P^2}{16b^2hkG_{13}} + \frac{P^2a^2}{16b^2h^3E_{11}} \times \left[5.42\left(\frac{h}{a}\right)\left(\frac{E_{11}}{E_{33}}\right)^{1/4} + 2.45\left(\frac{h}{a}\right)^2\left(\frac{E_{11}}{E_{33}}\right)^{1/2}\right], \tag{38}$$

$$G_{II}^{SLB} = \frac{9P^2a^2}{16b^2h^3E_{11}}. \tag{39}$$

These expressions are, apart from the last term in Eq. (38), equivalent to those provided by Yoon and Hong [15]. For the ELS specimen $M_1 = 0$ and $M_2 = Pa$. Using Eqs. (35) and (36) we obtain:

$$G_I^{ELS} = \frac{12P^2a^2}{4b^2h^3E_{11}} + \frac{P^2}{4b^2hkG_{13}} + \frac{P^2a^2}{4b^2h^3E_{11}} \times \left[5.42\left(\frac{h}{a}\right)\left(\frac{E_{11}}{E_{33}}\right)^{1/4} + 2.45\left(\frac{h}{a}\right)^2\left(\frac{E_{11}}{E_{33}}\right)^{1/2}\right], \tag{40}$$

$$G_{II}^{ELS} = \frac{9P^2a^2}{4b^2h^3E_{11}}. \tag{41}$$

The sum of Eqs. (40) and (41) results in Eq. (23). The mode ratio (G_I/G_{II}) has the same form in both specimens

$$\left(\frac{G_I}{G_{II}}\right) = \frac{4}{3} + \frac{1}{9}\left[\frac{1}{k}\frac{E_{11}}{G_{13}}\left(\frac{h}{a}\right)^2 + 5.42\left(\frac{h}{a}\right)\left(\frac{E_{11}}{E_{33}}\right)^{1/4} + 2.45\left(\frac{h}{a}\right)^2\left(\frac{E_{11}}{E_{33}}\right)^{1/2}\right]. \quad (42)$$

According to Eq. (42) if we let the crack length to approach infinity, the mode ratio tends to 4/3.

3. Finite element analysis

The FE analysis was carried out under plane stress condition using the code COSMOS/M 2.0. Through the experiments some accompanying effects were observed. According to this for both specimens two kinds of FE models were developed. Only the advanced models are detailed here. Note that plane stress condition is consistent only with beam formulation of the problems. FE analysis under plane strain condition was also performed. Since results showed less than 1% difference between the results of plane stress and plain strain models with respect to both the compliance and fracture energy, we provide only the results of plane stress finite element analysis.

3.1. SLB specimen

Using the three-point bending fixture, shown in Fig. 5 due to the cylindrical shape of the support blocks the geometrical parameters (a, L_1, L_2) of the system change. The details of the FE model are illustrated also in Fig. 5.

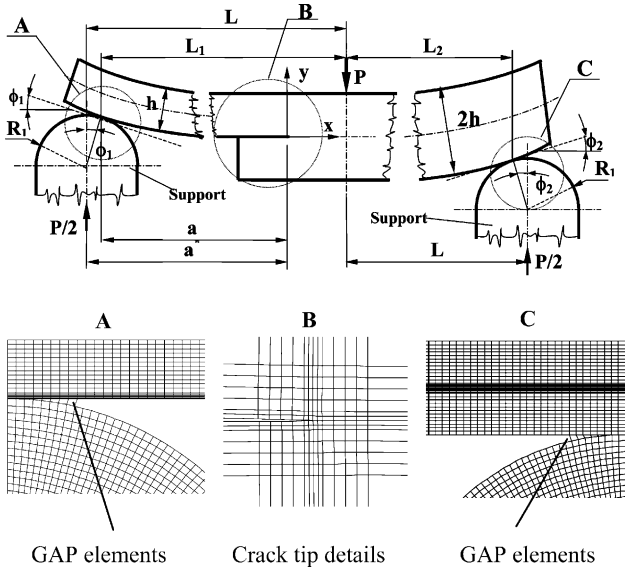

Fig. 5. Length shortening mechanism in the SLB specimen and details of the FE model.

The surroundings of the contact area between the specimen and the support blocks were meshed with linear (frictionless) node-to-node GAP elements. In the contact nodes of the blocks all the degrees of freedom were constrained. It was suitable to simulate the length shortening mechanisms. Similar corrections were implemented into Eqs. (20), (21), (38) and (39) based on simple beam theory and Fig. 5. Since our test fixture is non-standard this correction is not detailed here.

3.2. ELS specimen

In the case of the ELS specimen the large radius of the loading head should be considered. Fig. 6(a) shows that the point of contact between the specimen and the loading head changes with increasing load. The crack length was corrected based on the scheme in Fig. 6(a) using simple beam theory. The details of the correction are not given here, implementation was made into Eqs. (22), (23), (40) and (41). The FE models were constructed using the corrected crack lengths. The Saint Venant effect was considered. The clamped part had a length of 20 mm. The boundary conditions are shown in Fig. 6(b). Nodes, which are in contact with the clamping blocks, were constrained in the normal (y) direction. The center node at the clamped cross section was constrained only in the longitudinal (x) direction.

3.3. Energy release rate calculation

Figs. 5 and 6 show the FE mesh around the crack tip and the transition zone between the cracked and uncracked parts. At the crack tip singular elements were applied, the energy release rate components were calculated using the VCCT method [28]:

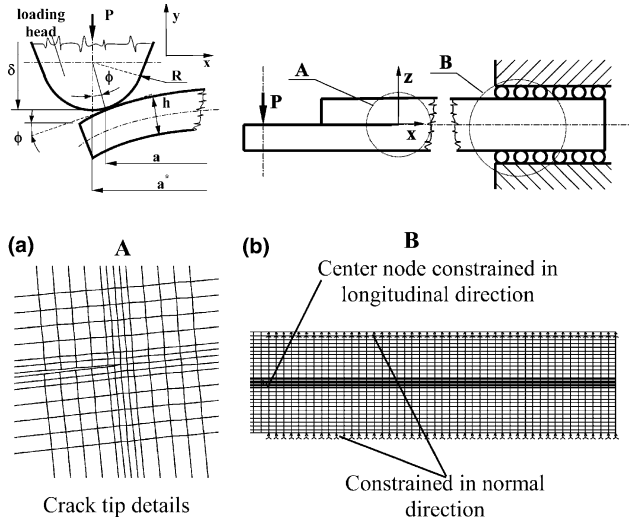

Fig. 6. Length shortening mechanism in the ELS specimen (a), details of the FE model (b).

$$G_{\mathrm{I}} = \frac{1}{2b\Delta a} F_y(v_1 - v_2), \tag{43}$$

$$G_{\mathrm{II}} = \frac{1}{2b\Delta a} F_x(u_1 - u_2), \tag{44}$$

where F_x, F_y are nodal forces at the crack tip, v_1, v_2, u_1, u_2 are nodal displacements from Δa distance to the crack tip and b is the specimen width. Crack tip elements with $\Delta a = 0.025$ mm were used (Figs. 5 and 6). The fracture energy was calculated by also the compliance calibration method.

4. Experiments

4.1. Data reduction

For both specimens we apply the compliance calibration (CC) method [2]. The compliance for mixed-mode I/II loading is

$$C = C_0 + ma^3. \tag{45}$$

The compliance was determined for each specimen at the point of fracture, and least square fitting was applied to find the coefficients C_0 and m in Eq. (45). The fracture work was obtained by using Eq. (2) for each crack length.

4.2. Experimental procedure

Unidirectional $[0°]_{14}$ glass/polyester laminates were manufactured in a special pressure block tool with nominal width of 20 mm, thickness of $2h = 6$ mm and $V_f = 43\%$. A nylon insert with thickness of 0.04 mm was placed at the midplane. The specimens were cut to the desired length and have been precracked in opening mode of about 5–10 mm by using a sharp blade. This involved a crack tip region full of pulled-out fibers but this effect was ignored. The flexural moduli was determined from a three-point bending test, which resulted $E_{11} = 33$ GPa. Other properties were predicted according to Thamm [34]: $G_{13} = 3$ GPa, $E_{33} = 7.2$ GPa and $v_{13} = 0.27$. The SLB test was performed in the same three-point bending fixture (see Fig. 7(a)) with span length of $2L = 151$ mm. The special fixture depicted in Fig. 7(b) was used to carry out the ELS test with full length of $L = 150$ mm. In order to avoid the effects of fiber-bridgings specimens with different crack lengths were prepared. SLB coupons with crack lengths from $a = 20$–75 mm with 5 mm increment were used. For the ELS specimen the former crack length range was improved from $a = 80$–140 mm with 10 mm increment. Tests were conducted under displacement control using an Amsler testing machine. Note that all fixtures were non-standard. Load-deflection data was recorded, the deflection was monitored by the dial gauge, shown in Fig. 7(a)–(b). Crack initiation/propagation was visually observable in the specimen boundaries.

5. Results and discussion

5.1. Load and deflection

For both tests linear load-deflection curves were recorded up to fracture as shown by Fig. 8(a)–(b). Figs. 9 and 10 illustrate the critical load and the critical specimen displacement against the crack length. The displacements calculated from the beam and FE model are also plotted. The critical load shows hyperbolic, while

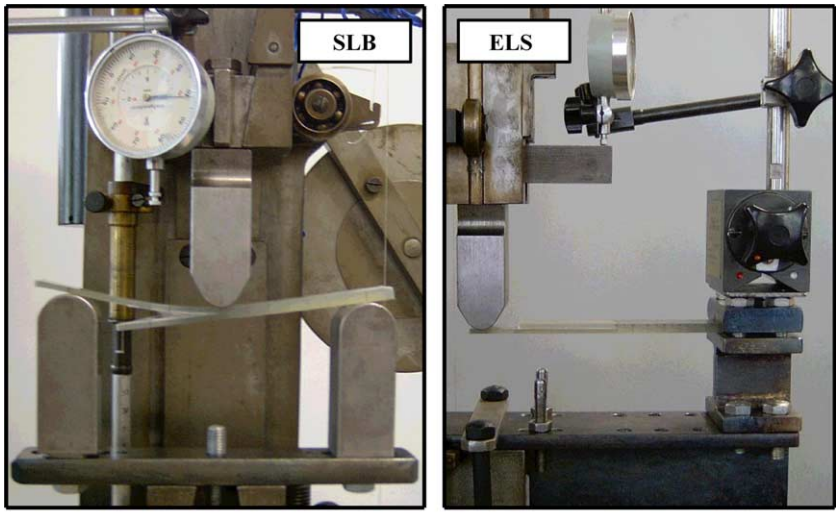

Fig. 7. Experimental setups for mixed-mode I/II testing.

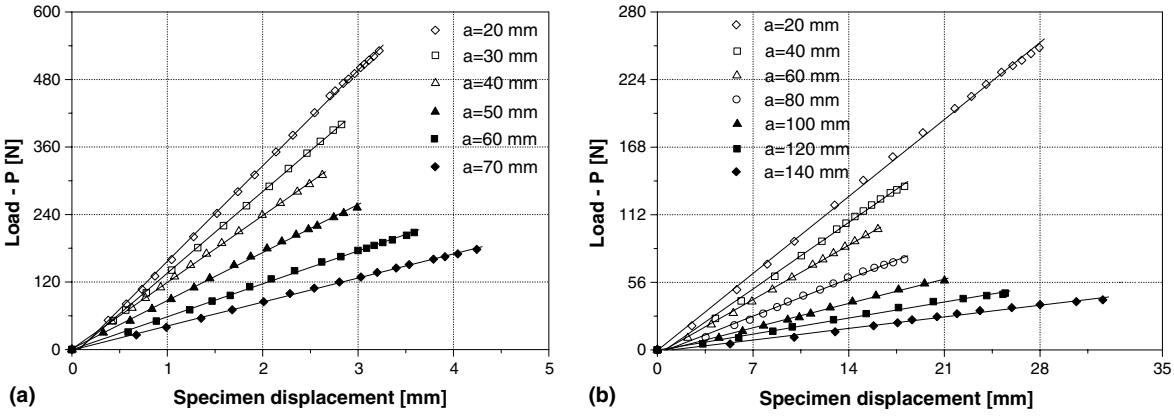

Fig. 8. Load–displacement curves up to fracture, SLB specimen (a), ELS specimen (b).

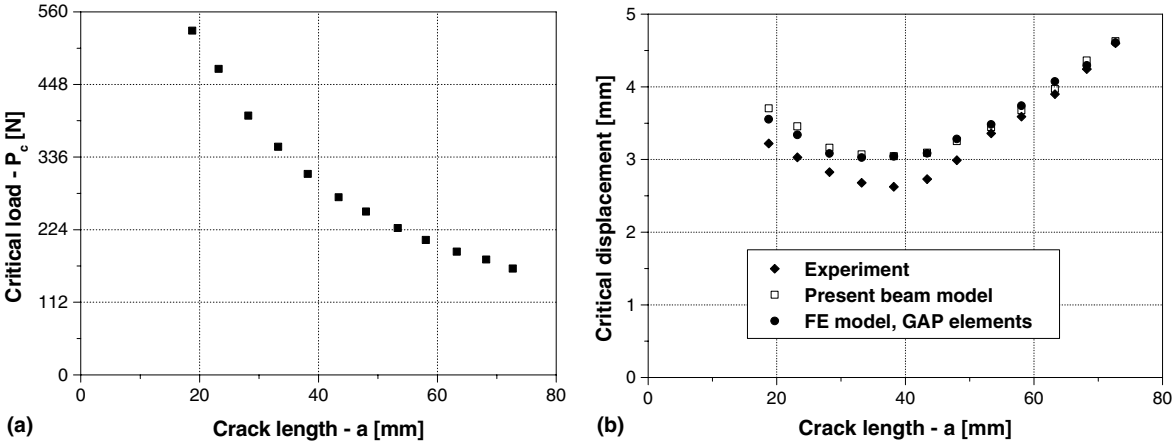

Fig. 9. The critical load (a) and critical displacement (b) against the crack length (SLB specimen).

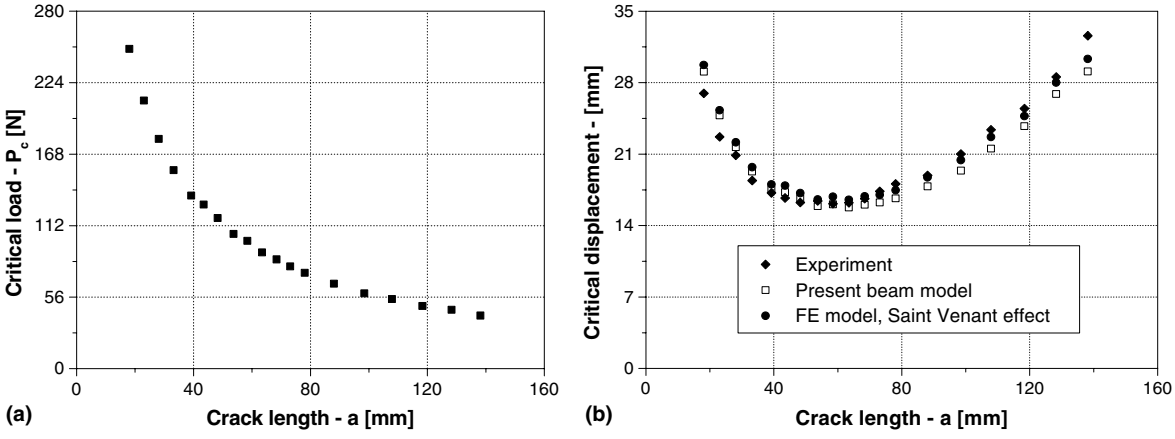

Fig. 10. The critical load (a) and critical displacement (b) against the crack length (ELS specimen).

the displacement has parabolic relation for both specimens. Considering the points in Fig. 9(b) both the beam and FE models overpredict the experimental values over the interval, however the differences decrease with increasing crack length. No large displacements were experienced through the SLB test, which indicates that the chosen crack interval ($0.13\times 2L < a < 0.49\times 2L$) is reasonable for fracture investigation using linear beam theories. For comparison Korjakin et al. [23] used glass/epoxy MMF specimens (2L = 76 mm) within the crack

length range of $0.25\times2L<a<0.45\times2L$. In the case of the ELS specimen the beam model shows overpredictions until $a=60$ mm, and after the beam displacements fall below the experimental ones (Fig. 10(b)). The FE model slightly overpredicts the experimental values. It is clear from Fig. 10(b) that large displacements occur. For a useful crack length interval the lower bound is $a=35$ mm, the upper one is $a=120$ mm (refer to Fig. 10(b)), writing simply: $0.23L<a<0.8L$. Hashemi et al. [7,8] performed experiments on mixed-mode carbon/PEEK and PES ELS specimens with $L=135$ mm and $L=120$ mm, respectively. The relevant crack length ranges were $0.5L<a<0.8L$ and $0.2L<a<0.7L$, respectively. Our suggested interval agrees well with those reported in their work.

5.2. Compliance and fracture energy

The compliance and fracture resistance curves are illustrated in Fig. 11 for the SLB specimens. The correlation between model (Eqs. (20) and (21)) and experiment was found to be quite good considering both quantities, but it should be noted that Eq. (20) slightly overestimates the experimental points. The results of the ELS test follow similar trends, as shown in Fig. 12. The advanced beam model overestimates the measured compliance values (Fig. 12(a)) until $a=60$ mm, overall Eq. (22) shows good agreement with the experiments. The fracture energy values by CC method can be seen in Fig. 12(b) for the ELS test. The correspondence between model (Eq. (23)) and experiment was not as good as in the case of the SLB test. The CC method indicates averaged steady state value of $G_{I/II,ss,init}=645$ J/m^2 for both tests. Advanced beam equations give $G_{I/II,ss,init}=623$ J/m^2 plateau value for the SLB and $G_{I/II,ss,init}=576$ J/m^2 for the ELS specimen (refer to Figs. 11(b) and 12(b)).

Since the MMF specimen is quite similar to the SLB one, and both produce the same mode ratio ($G_I/G_{II}=4/3$) based on simple beam theory we provide comparison between our experimental work and those by Albertsen et al. [22] and Korjakin et al. [23]. The former work reported $G_{I/II,init}=145$ J/m^2 initiation and $G_{I/II,ss}=330$ J/

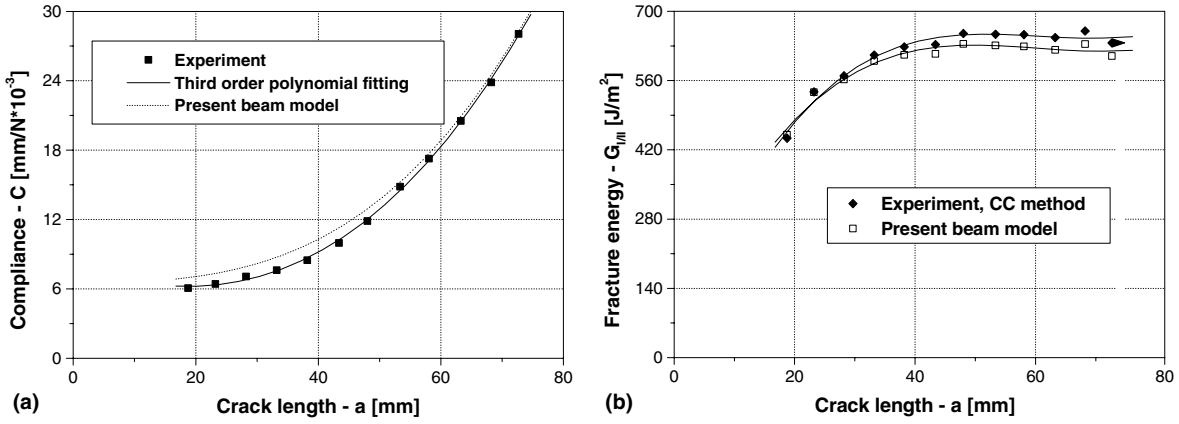

Fig. 11. Compliance (a) and values of the initiation fracture energy (b) against the crack length (SLB specimen).

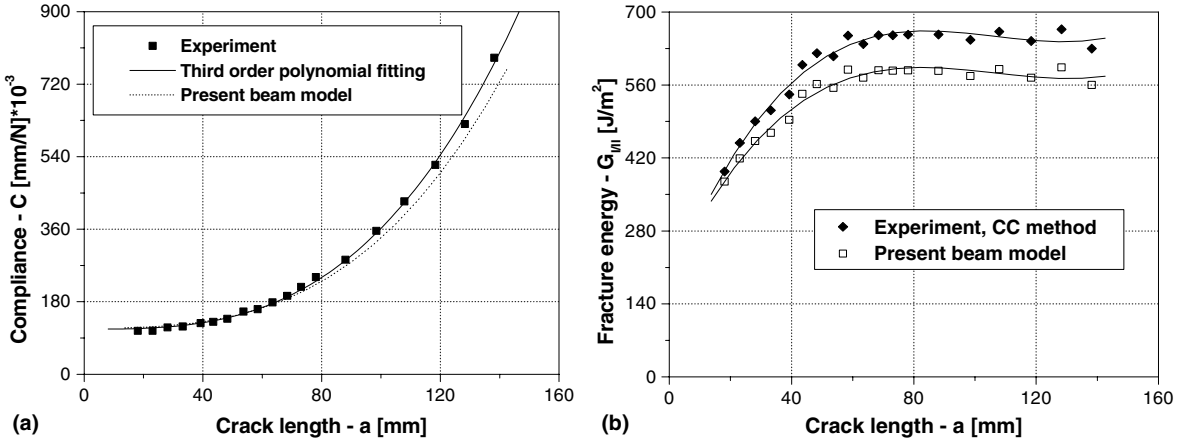

Fig. 12. Compliance (a) and values of the initiation fracture energy (b) against the crack length (ELS specimen).

m^2MMF specimens. In the later work the relevant quantities were $G_{I/II,init} = 456$ J/m^2 and $G_{I/II,ss} = 525$ J/m^2 for glass/epoxy MMF specimens. Similar *R*-curves were obtained by Hashemi et al. [7] for the ELS specimen, who determined (based on propagation tests) $G_{I/II,init} = 1200$ J/m^2 initiation toughness and $G_{I/II,ss} = 1480$ J/m^2 plateau value using PES ELS specimens. The same authors reported $G_{I/II,init} = 1510$ J/m^2 and $G_{I/II,ss} = 1810$ J/m^2 values for carbon/PEEK ELS specimens [8]. Fiber-bridging was observed in all these studies. However the current study presents only initiation values, the behavior is similar to results previously published on similar systems.

The compliances calculated from the beam and FE models of the SLB specimen are listed in Table 1. While the simple FE model overpredicts the experimental compliance values (refer to Fig. 11(a)), the advanced FE model partly eliminates the overestimations. The Timoshenko beam model and elastic foundation show negligible compliance contributions. The fracture energy values are summarized also in Table 1. The simple FE model seems to be again inaccurate, the advanced model shows better correlation with the values obtained from CC method (refer to Fig. 11). The Timoshenko beam model supports the fracture energy with very small value. The contribution of elastic foundation decays subsequently, but provides reasonable values at each crack length (last column in Table 1).

Table 2 presents the compliances obtained from the ELS test. The simple FE model shows higher compliance values in comparison with the experimental points until the crack length of $a = 60$ mm, and has lower values beyond this crack length (Table 2, second column). The FE model including Saint Venant effect shows similar behavior with more significant overpredictions at shorter crack lengths. The various contributions from beam theories are collected in the last three columns of Table 2. Transverse shear can be neglected. In contrast the Saint Venant effect is a somewhat larger contribution. The small deviation in Table 2 is due to crack length correction. The contribution of the EFM to the full compliance shows increasing values as the crack length increases. The fracture energy by FE and beam analysis is presented in Table 3 for the ELS specimen. The simple FE model and the one including Saint Venant effect give essentially the same results with steady-state fracture energy value of $G_{I/II,ss,init} = 606$ J/m^2. The effect of transverse shear on the specimen's strain energy release rate can be neglected, as demonstrated in Table 3. The EFM shows meaningful values at the beginning phase ($a = 20$–50 mm), as shown by the last column.

5.3. Mode-mixity results

The mode-I, mode-II energy release rate components and the mode ratio were calculated using Eqs. (38)–(42). Comparison was made with the results of the VCCT

Table 1
Compliances and fracture energies by finite element and beam analysis (SLB specimen)

a^* (mm)	C_{Fem} (mm/N$\times 10^{-3}$)	C_{FE-GAP} (mm/N$\times 10^{-3}$)	C_{SB} (mm/N$\times 10^{-3}$)	C_{TIM} (mm/N$\times 10^{-3}$)	C_W (mm/N$\times 10^{-3}$)	$G_{II,FE}$ (J/m^2)	$G_{II,FE-GAP}$ (J/m^2)	$G_{II,SB}$ (J/m^2)	$G_{II,TIM}$ (J/m^2)	$G_{II,W}$ (J/m^2)
20	7.55	6.69	6.79	0.15	0.04	491.96	430.05	417.30	6.32	26.91
25	8.08	7.08	7.11	0.15	0.06	595.69	520.72	505.62	5.00	25.85
30	8.81	7.71	7.67	0.16	0.08	631.75	552.24	536.52	3.59	22.25
35	9.85	8.60	8.45	0.16	0.11	678.52	593.13	576.46	2.78	20.10
40	11.15	9.82	9.51	0.16	0.15	696.59	608.93	591.96	2.16	17.81
45	12.81	11.26	10.93	0.17	0.19	701.85	613.53	596.61	1.69	15.71
50	14.92	13.03	12.51	0.17	0.23	726.69	635.24	617.96	1.43	14.64
55	17.40	15.38	14.76	0.18	0.28	725.09	633.84	616.82	1.15	13.09
60	20.32	17.98	17.17	0.18	0.33	724.23	633.09	616.07	0.97	11.98
65	23.51	21.44	20.34	0.19	0.38	717.52	627.22	610.29	0.81	10.87
70	27.90	24.13	23.87	0.19	0.45	732.33	640.16	622.76	0.71	10.26
75	32.38	28.10	27.53	0.19	0.50	705.63	616.83	599.92	0.60	9.27

a^* – measured crack length; C_{FE} – plane stress FE model; C_{FE-GAP} – plane stress FE model including geometry correction; C_{SB} – contribution of the simple beam model; C_{TIM} – contribution of the Timoshenko beam model; C_W – contribution of the Winkler foundation model; $G_{II,FE}$ – plane stress FE model, CC method; $G_{II,FE-GAP}$ – plane stress FE model including geometry correction, CC method; $G_{II,SB}$ – contribution of the simple beam model; $G_{II,TIM}$ – contribution of the Timoshenko beam model; $G_{II,W}$ – contribution of the Winkler foundation model.

Table 2
Compliances by finite element and beam analysis (ELS specimen)

a^* (mm)	C_{Fem} (mm/N$\times 10^{-3}$)	C_{Fem-SV} (mm/N$\times 10^{-3}$)	C_{SB} (mm/N$\times 10^{-3}$)	C_{TIM} (mm/N$\times 10^{-3}$)	C_{SV} (mm/N$\times 10^{-3}$)	C_W (mm/N$\times 10^{-3}$)
20	104.82	118.68	102.71	0.58	12.65	0.15
30	109.21	123.06	106.80	0.62	12.69	0.33
40	119.15	133.08	115.51	0.66	12.72	0.62
50	131.69	145.54	126.90	0.69	12.72	0.91
60	154.30	168.24	146.03	0.72	12.71	1.32
70	183.33	197.27	172.37	0.76	12.70	1.79
80	218.97	232.76	206.33	0.79	12.68	2.32
90	267.62	281.48	251.77	0.83	12.68	2.93
100	332.02	345.95	311.37	0.86	12.67	3.65
110	402.09	415.94	377.31	0.90	12.65	4.37
120	490.60	504.46	465.54	0.93	12.65	5.24
130	595.05	608.91	564.79	0.97	12.63	6.14
140	716.67	730.57	680.33	1.00	12.62	7.11

C_{Fem} – plane stress FE model; C_{Fem-SV} – plane stress FE model including Saint Venant effect; C_{SB} – contribution of the simple beam model; C_{TIM} – contribution of the Timoshenko beam model; C_{SV} – contribution of the Saint Venant effect; C_W – contribution of the Winkler foundation model.

Table 3
Fracture energy values by finite element and beam analysis (ELS specimen)

a^* (mm)	$G_{I/II,Fem}$ (J/m^2)	$G_{I/II,Fem-SV}$ (J/m^2)	$G_{I/II,SB}$ (J/m^2)	$G_{I/II,TIM}$ (J/m^2)	$G_{I/II,W}$ (J/m^2)
20	365.71	365.70	345.79	5.61	23.22
30	455.00	454.98	430.21	2.90	17.97
40	502.90	502.88	475.50	1.64	13.96
50	576.29	576.27	544.90	1.25	12.90
60	607.57	607.56	574.48	0.89	11.15
70	608.19	608.17	575.06	0.65	9.50
80	609.36	609.35	576.17	0.50	8.31
90	609.50	609.48	576.30	0.40	7.35
100	600.02	600.00	567.34	0.31	6.45
110	614.59	614.57	581.11	0.27	6.02
120	597.86	597.84	565.29	0.21	5.33
130	618.89	618.87	585.18	0.19	5.09
140	584.43	584.41	552.59	0.15	4.46

$G_{I/II,Fem}$ – plane stress FE model, CC method; $G_{I/II,Fem-SV}$ – plane stress FE model including Saint Venant effect, CC method; $G_{I/II,SB}$ – contribution of the simple beam model; $G_{I/II,TIM}$ – contribution of the Timoshenko beam model; $G_{I/II,W}$ – contribution of the Winkler foundation model.

Table 4
Mode partitioning by finite element and beam analysis (SLB specimen)

a^* (mm)	$G_{I,FE}$ (J/m^2)	$G_{II,FE}$ (J/m^2)	$(G_I/G_{II})_{FE}$ (−)	$G_{I,B}$ (J/m^2)	$G_{II,B}$ (J/m^2)	$(G_I/G_{II})_B$ (−)
20	263.74	219.57	1.201	271.69	178.84	1.519
25	319.45	283.79	1.126	319.77	216.70	1.476
30	329.12	296.53	1.110	332.43	229.94	1.446
35	349.05	326.77	1.068	352.28	247.05	1.426
40	354.35	342.95	1.033	358.23	253.70	1.412
45	352.02	341.32	1.031	358.32	255.69	1.401
50	358.67	358.29	1.001	369.19	264.84	1.394
55	366.94	357.47	1.027	366.71	264.35	1.387
60	355.77	359.57	0.989	364.99	264.03	1.382
65	365.40	357.40	1.022	360.41	261.55	1.378
70	333.53	334.11	0.998	366.84	266.90	1.374
75	293.07	317.79	0.922	352.68	257.11	1.372

$G_{I,FE}$ – mode-I component, FE model, VCCT method; $G_{II,FE}$ – mode-II component, FE model, VCCT method; $(G_I/G_{II})_{FE}$ – mode ratio, FE analysis; $G_{I,B}$ – mode-I component, beam model; $G_{II,B}$ – mode-II component, beam model; $(G_I/G_{II})_B$ – mode ratio, beam model.

method. In Tables 4 and 5 the mode-I, mode-II components and the mode ratio are collected for each crack length. The VCCT method indicates that the mode ratio gradually decreases from 1.2 to 0.92 in the SLB (Table 4), and from 1.19 to 0.95 in the case of the ELS specimen (Table 5). The beam model shows that in the case of the SLB the mode ratio decreases from 1.52 to 1.37, while in the case of the ELS specimen it de-

Table 5
Mode partitioning by finite element and beam analysis (ELS specimen)

a^* (mm)	$G_{I,FE}$ (J/m^2)	$G_{II,FE}$ (J/m^2)	$(G_I/G_{II})_{FE}$ (−)	$G_{I,B}$ (J/m^2)	$G_{II,B}$ (J/m^2)	$(G_I/G_{II})_B$ (−)
20	297.86	250.72	1.188	226.42	148.19	1.528
30	311.26	293.41	1.061	266.70	184.38	1.447
40	310.95	303.77	1.024	287.32	203.79	1.410
50	354.07	353.30	1.002	325.52	233.53	1.394
60	371.67	371.54	1.000	340.32	246.20	1.382
70	368.74	369.45	0.998	338.75	246.45	1.375
80	355.12	367.12	0.967	338.05	246.93	1.369
90	353.31	365.62	0.966	337.06	246.99	1.365
100	346.86	358.63	0.967	330.96	243.14	1.361
110	354.75	367.27	0.966	338.35	249.05	1.359
120	340.97	353.48	0.965	328.57	242.27	1.356
130	351.91	365.76	0.962	339.66	250.79	1.354
140	327.65	344.97	0.950	320.38	236.83	1.353

$G_{I,FE}$ – mode-I component, FE model, VCCT method; $G_{II,FE}$ – mode-II component, FE model, VCCT method; $(G_I/G_{II})_{FE}$ – mode ratio, FE analysis; $G_{I,B}$ – mode-I component, beam model; $G_{II,B}$ – mode-II component, beam model; $(G_I/G_{II})_B$ – mode ratio, beam model.

creases from 1.53 to 1.35. This feature is mainly caused by elastic foundation, since the effect of transverse shear is negligible. The FE and beam models indicate similar crack length dependence. Due to the mixed-mode condition similar effect related to elastic foundation can arise from the mode-II component. Further work is required to investigate this problem. The VCCT method gives higher fracture energy values in comparison with the beam model at each crack length (Tables 4 and 5), as experienced by even Ducept et al. [28] in MMB specimens.

6. Conclusions

A set of equations was developed based on Timoshenko beam theory and Winkler foundation analysis. The beam analysis showed that the compliance of both specimens follows a full third order polynomial. FE models were constructed using plane stress elements. The results of the theoretical models were compared with the relevant experimental data. The agreement between them was quite good. In the case of the SLB the correlation was found to be better than in the case of the ELS specimen. The SLB and ELS configurations prove very similar fracture behavior in the chosen crack intervals. The Winkler foundation model seems to be useful tool to obtain improved solution for mixed-mode delamination specimens. The mode-mixity was also investigated incorporating transverse shear, elastic foundation effects and the VCCT method. The crack length dependence of the mode ratio was found to be similar in both specimens.

Based on our experiments the steady-state value of $G_{I/II,ss,init} = 645$ J/m^2 was obtained for the initiation fracture energy from both tests. Our experimental fracture toughness data was compared with previous ones carried out on MMF and ELS specimens. Similar behavior was found. During the SLB test no large displacements were observed. This indicates that the used crack interval is reasonable for fracture testing, linear beam theories can be applied for analysis. In contrast the ELS test showed relatively large displacements if the crack length was outside the range of $0.23L < a < 0.8L$.

Acknowledgement

This research work was supported by the fund OTKA T037324. The authors grateful to Alfredo Balacó de Morais, Tonny Nyman and Gábor M. Vörös who have given meaningful recommendations, and also to Frigyes Thamm for his helps in the experiments. I am grateful to my father for his patience in manufacturing the experimental tools. We wish to thank Tonny Nyman for providing [15] and Barry D. Davidson for providing [17–19].

Appendix A. Bending and shear compliances, SLB specimen

The bending and shear compliances of the cracked (1) and uncracked (2) portions of unidirectional symmetric SLB specimens are:

$$d_{11,1} = \frac{12}{bh^3E_{11}}, \quad a_{55,1} = \frac{1}{bhG_{13}}, \tag{A.1a}$$

$$d_{11,2} = \frac{3}{2bh^3E_{11}}, \quad a_{55,2} = \frac{1}{2bhG_{13}}. \tag{A.1b}$$

Appendix B. Displacement functions, boundary and matching conditions, ELS specimen

The generalized Krulov-functions are [26]:

$$V_1(x) = \cosh(\zeta x)\cos(\zeta x), \tag{B.1a}$$

$$V_2(x) = \frac{1}{2}[\cosh(\zeta x)\sin(\zeta x) + \sinh(\zeta x)\cos(\zeta x)], \quad \text{(B.1b)}$$

$$V_3(x) = \frac{1}{2}\sinh(\zeta x)\sin(\zeta x), \quad \text{(B.1c)}$$

$$V_4(x) = \frac{1}{4}[\cosh(\zeta x)\sin(\zeta x) - \sinh(\zeta x)\cos(\zeta x)]. \quad \text{(B.1d)}$$

The complete deflection functions of the upper and lower sub-beams of the uncracked region ($0 \leqslant x \leqslant c$) are:

$$w_{u2}(x) = c_5 + c_6 x + c_7 x^2 + c_8 x^3 - \left(\frac{\beta_u}{\beta_l}\right)^4 [c_9 V_1(x) + c_{10} V_2(x) + c_{11} V_3(x) + c_{12} V_4(x)], \quad \text{(B.2a)}$$

$$w_{l2}(x) = c_5 + c_6 x + c_7 x^2 + c_8 x^3 + [c_9 V_1(x) + c_{10} V_2(x) + c_{11} V_3(x) + c_{12} V_4(x)], \quad \text{(B.2b)}$$

where

$$\zeta = \left(\beta_u^4 + \beta_l^4\right)^{1/4}. \quad \text{(B.2c)}$$

The boundary conditions can be written as:

$$w_{u2}(c) = 0, \quad w_{l2}(c) = 0, \quad \text{(B.3a)}$$

$$w'_{u2}(c) = 0, \quad w'_{l2}(c) = 0. \quad \text{(B.3b)}$$

The matching conditions considering Eq. (14) are:

$$w_{u1}(0) = w_{u2}(0), \quad w_{l1}(0) = w_{l2}(0), \quad \text{(B.4a)}$$

$$w'_{u1}(0) = w'_{u2}(0), \quad w'_{l1}(0) = w'_{l2}(0), \quad \text{(B.4b)}$$

$$w''_{u1}(0) = \left(\frac{h_u^2 + 3h_l^2}{h_u^2}\right) w''_{u2}(0),$$
$$w''_{l1}(0) = \left(\frac{h_l^2 + 3h_u^2}{h_l^2}\right) w''_{l2}(0), \quad \text{(B.4c)}$$

$$w'''_{u1}(0) = \left(\frac{h_u^2 + 3h_l^2}{h_u^2}\right) w'''_{u2}(0),$$
$$w'''_{l1}(0) = \left(\frac{h_l^2 + 3h_u^2}{h_l^2}\right) w'''_{l2}(0). \quad \text{(B.4d)}$$

References

[1] Olsson R. A simplified improved beam analysis of the DCB specimen. Compos Sci Technol 1992;43:329–38.

[2] Ozdil F, Carlsson LA. Beam analysis of angle-ply laminate DCB specimens. Compos Sci Technol 1999;59:305–15.

[3] Wang Y, Williams JG. Corrections for mode II fracture toughness specimens of composite materials. Compos Sci Technol 1992;43:251–6.

[4] Ozdil F, Carlsson LA, Davies P. Beam analysis of angle-ply laminate end-notched flexure specimens. Compos Sci Technol 1998;58:1929–38.

[5] Carlsson LA, Gillespie JW, Pipes RB. On the analysis and design of the end notched flexure (ENF) specimen for mode II testing. J Compos Mater 1986;20:594–604.

[6] Schuecker C, Davidson BD. Evaluation of the accuracy of the four-point bend end-notched flexure test for mode II delamination toughness determination. Compos Sci Technol 2000;60:2137–46.

[7] Hashemi S, Kinloch J, Williams JG. The effects of geometry, rate and temperature on mode I, mode II and mixed-mode I/II interlaminar fracture toughness of carbon–fibre/poly (ether–ether ketone) composites. J Compos Mater 1990;24:918–56.

[8] Hashemi S, Kinloch J, Williams JG. Mechanics and mechanisms of delamination in a poly (ether sulphone)-fibre composite. Compos Sci Technol 1990;37:429–62.

[9] Ozdil F, Carlsson LA. Beam analysis of angle-ply laminate mixed-mode bending specimens. Compos Sci Technol 1999;59:937–45.

[10] Reeder JR, Crews JR. Mixed-mode bending method for delamination testing. AIAA J 1990;28:1270–6.

[11] Chen JH, Sernow R, Schulz G, Hinrichsen G. A modification of the mixed-mode bending test apparatus. Compos Part A: Appl Sci Manufact 1999;30:871–7.

[12] Reyes G, Cantwell WJ. The mechanical properties of fibre-metal laminates based on glass fibre reinforced polypropylene. Compos Sci Technol 2000;60:1085–94.

[13] Dahlen C, Springer GS. Delamination growth in composites under cyclic loads. J Compos Mater 1994;28:732–81.

[14] Yan A-M, Marechal E, Nguyen-Dang H. A finite element model of mixed-mode delamination in laminated composites with an R-curve effect. Compos Sci Technol 2001;61:1413–27.

[15] Yoon SH, Hong CS. Modified end notched flexure specimen for mixed mode interlaminar fracture in laminated composites. Int J Fracture 1990;43:R3–9.

[16] Davidson BD, Krüger R, König M. Three-dimensional analysis of center-delaminated unidirectional and multidirectional single-leg bending specimens. Compos Sci Technol 1995;54:385–94.

[17] Davidson BD, Sundararaman V. A single leg bending test for interfacial fracture toughness determination. Int J Fracture 1996;78:193–210.

[18] Davidson BD, Fariello PL, Hudson RC, Sundararaman V. Accuracy assessment of the singular-field-based mode-mix decomposition procedure for the prediction of delamination. Composite Materials: Testing and Design. vol. 13, ASTM STP 1242; 1997. p.109–28.

[19] Davidson BD, Gharibian SJ, Yu L. Evaluation of energy release rate-based approaches for predicting delamination growth in laminated composites. Int J Fracture 2000;105:343–65.

[20] Davidson BD, Koudela KL. Influence of the mode mix of precracking on the delamination toughness of laminated composites. J Reinforced Plast Compos 1999;18:1408–14.

[21] Tracy GD, Feraboli P, Kedward KT. A new mixed mode test for carbon/epoxy composite systems. Compos Part A: Appl Sci Manufact 2003;34:1125–31.

[22] Albertsen H, Ivens J, Peters P, Wevers M, Verpoest I. Interlaminar fracture toughness of CFRP influenced by fiber surface treatment: Part 1. Experimental results. Compos Sci Technol 1995;54:133–45.

[23] Korjakin A, Rikards R, Buchholz F-G, Wang H, Bledzki AK, Kessler A. Comparative study of interlaminar fracture toughness of GFRP with different fiber surface treatments. Polym Compos 1998;19:793–806.

[24] Lai Y-H, Rakestraw MD, Dillard DA. The cracked lap shear specimen revisited – a closed form solution. Int J Solid Struct 1996;33:1725–43.

[25] Broek D. Elementary engineering fracture mechanics. The Hauge: Martinus Nijhoff Publishers; 1982.
[26] Ponomarjov Sz. D. Szilárdsági számítások a gépészetben, 2. Kötet. Rudak, rugók. Mûszaki Könyvkiadó, Budapest; 1968.
[27] Horgan CO. On Saint-Venant's principle in plane anisotropic elasticity. J Elasticity 1972;2:169–80.
[28] Ducept F, Gamby D, Davies P. A mixed-mode failure criterion derived from tests of symmertic and asymmetric specimens. Compos Sci Technol 1999;59:609–19.
[29] Williams JG. On the calculation of energy release rates for cracked laminates. Int J Fracture 1988;36:101–19.
[30] Suo Z, Hutchinson JW. Interface crack between two elastic layers. Int J Fracture 1990;43:1–18.
[31] Bruno D, Greco F. Mixed mode delamination in plates: a refined approach. Int J Solids Struct 2001;38:9149–77.
[32] Sundararaman V, Davidson BD. An unsymmetric end-notched flexure test for interfacial fracture toughness determination. Engineering Fracture Mech 1998;60:361–77.
[33] Sundararaman V, Davidson BD. An unsymmetric double cantilever beam test for interfacial fracture toughness determination. Int J Solids Struct 1997;34:799–817.
[34] Thamm F. Mûanyagok szilárdságtana II. Budapest; 1985.